Abstract #: 2282

Optics of the offshore Columbia River plume in spring-summer

Gonzalo S. Saldías*, R. Kipp Shearman, John A. Barth, Nicholas Tiffilaro, Curtiss O. Davis

College of Earth, Ocean, and Atmospheric Sciences, Oregon State University, Corvallis, Oregon.
* gsaldias@coas.oregonstate.edu

Introduction

Oceanic optical properties can be influenced by several biological, geological, and physical processes. In this regard, the influence of rivers and estuaries is particularly important as these can deliver very large sediment loads [Milliman and Meade, 1983], in conjunction with terrestrial particulate and dissolved matter [e.g. Del Castillo et al., 1999]. As result, most river plumes have a contrasting green-brownish color, which makes them readily distinguishable from ambient waters through satellite images of ocean color [e.g. Thomas and Weatherbee, 2006]. However, data derived solely from satellite imagery do not provide any insight about the vertical structure (i.e. stratification, plume thickness) and/or the vertical distribution of optical properties in the water column. In situ observations are, consequently, essential part of a monitoring program in order to assess river plume signals from satellite data, and also to identify variations in the plume's vertical structure in response to physical forcing (e.g. wind stress, surface currents, river flow).

The Columbia River (CR) delivers about three quarters of the total freshwater input of the northwest United States [Barnes et al., 1972]. The seasonality of the river flow has been widely described – high discharge occurs during winter and spring (~10,000-15,000 $m^3 s^{-1}$), whereas the minimum flow takes place in late summer (~3,000 $m^3 s^{-1}$) [e.g. Morgan et al., 2005]. The resultant plume can be transported in different directions according to the interplay of the river flow and the seasonal pattern of wind stress and surface circulation [Hickey et al., 1998]. Also, its high nutrient content would enhance local production at multiple trophic levels [Kudela et al., 2010], by which the fate of the plume is crucial for the biogeochemistry of the coastal ocean. In terms of its optical properties, an early study by Pak et al. [1970] showed that the plume's light-scattering field is consistent with its low salinity (~32) along the plume's main axis, and extending ~190 km south from its origin in summer. Further south, the tongue-shaped feature of the plume is lost presumably due to higher rates of particle sinking [Pak et al., 1970]. Recently, few efforts have quantified the particle resuspension and dynamics in the near-field region (next to the river mouth) [Nowacki et al., 2012; Spahn et al., 2009], yet little is known in the plume's far-field.

Remote sensing studies have shown the CR plume is frequently found off Oregon in spring-summer [Fiedler and Laurs, 1990; Thomas and Weatherbee, 2006]. Nonetheless, satellite observations have only been complemented with in situ data in the near-field area [Palacios et al., 2009; Palacios et al., 2012], and a long-term monitoring study in the far-field is still missing. Since the CR plume scattering signature changes in the alongshore direction [Pak et al., 1970], it is absolutely necessary to take optical measurements in the far-field, and for an extended period of time, to try to understand the role of the plume in the optics of the northern California Current System. This task is challenging and very costly through traditional shipboard surveys, by which the use of autonomous underwater gliders becomes crucial for maintaining a persistent monitoring of the optical and hydrographic conditions in the region. Here, we used observations from slocum gliders and MODIS ocean color imagery from 7 upwelling seasons (2006-2012) to study the optics of the offshore CR plume off Newport, Oregon. The unusual high resolution of our long-term synoptic glider transects provides a unique opportunity to study the optics of the offshore CR plume. Our primary objective is to provide a descriptive characterization of the optical properties of coastal waters off Newport as they are modified by the presence of the CR plume. To our knowledge, there is no previous study characterizing the optical properties of the CR plume using fine-scale measurements from underwater gliders.

Methods

Glider measurements

Cross-shore repeated glider surveys off Newport, Oregon (Fig. 1), have been conducted from April 2006 to date by the Oregon State University Glider Research Group using a fleet of slocum gliders (http://www.webbresearch.com/slocumglider.aspx) [Schofield et al., 2007]. Here, we used all data spanning the upwelling seasons of 7 years (2006-2012). The glider sections from 2013 are not included in the present study as they are significantly reduced in comparison to previous years. In general, glider surveys collected data very frequently during spring-summer. The gliders recorded standard hydrographic variables; pressure, temperature, conductivity, and dissolved oxygen, and a big part of them also measured optically derived Colored Dissolved Organic Matter (CDOM), backscatter, and chlorophyll. A total of 285 cross-shelf sections were conducted between April 2006 and December 2012, 201 (70%) of them during spring-summer (Apr-Sep) months. The sections are about 70-75 km long, generally expanding from ~30 m to the 1000-2000 m isobath in ~5 days. These gliders are operational in waters up to 200 m. It is worth mentioning that before the start of our glider endurance line in 2006, the NH line was historically sampled via bi-monthly oceanographic cruises sampling at fixed stations [Huyer et al., 2007]. Hence, our glider sections present the highest spatio-temporal resolution achieved in the region.

The optical measurements are made through two WETLabs Inc Environmental Characterization Optics (ECO) Pucks mounted in the bottom of the gliders and facing downwards. The measurements are in the form of raw voltages which are converted to the desired quantity by using the following linear relationship:

$[\beta(\theta_c)$, Chl, CDOM$]$ = scale factor * (output – dark counts)

scale factor = x / (output – dark counts), for the case of Chl ($\mu g\ l^{-1}$) and CDOM (ppb)

scale factor = experimental ($b_b(\lambda)$ / counts) * theoretical ($\beta(\theta_c) / b_b(\lambda)$), for the case of total volume scattering $\beta(\theta_c)$ ($m^{-1}\ sr^{-1}$)

where x is a known concentration of the constituent (Chl or CDOM), $b_b(\lambda)$ is the total backscattering coefficient (m^{-1}), and the dark counts is the signal in the absence of light. From the total volume scattering is possible to obtain the volume scattering of particles (β_p) by subtracting the volume scattering of water (β_w) [Morel, 1974]. Then the β_p is used to compute the particulate backscatter coefficients (b_{bp}; m^{-1}) and total backscattering coefficients (b_b; m^{-1}) following Boss and Pegau [2001]. A detailed description of the backscattering computation is found in the official WETLabs website (http://www.wetlabs.com/eco-triplet). Additional information about manufacturer calibration of Eco Pucks' fluorometric measurements is found in Cetinić et al. [2009].

MODIS imagery

High-resolution ocean color imagery from MODIS-Aqua and MODIS-Terra were used to detect and track the surface signature of the plume during the upwelling season. All satellite images, for the years 2006-2012, were processed using the NASA's software SeaDAS (SeaWIFS Data Analysis System) for the coastal region off Oregon limited by the latitudes 42˚ and 47˚ N and longitudes 128˚ and 123˚ W. The processing was achieved using default atmospheric corrections (Gordon, 1997) and flags. Although it is well recognized the black pixel assumption no longer hold by using NIR (near infrared) bands for correction in turbid waters, and consequently the use of other bands as SWIR (short wave infrared) are recommended [Wang and Shi, 2007], we opted for maintaining default (NIR) settings for two reasons; 1) The implementation of SWIR bands in SeaDAS increased the noise and missing data of final products in our region of study, and 2) the offshore CR plume shows a lower level of turbidity as compared to the near-field area. The processing of the satellite imagery included all the visible spectrum of normalized water-leaving radiance (nLw(λ); at 412, 443, 469, 488, 531, 547, 555, 645, 667, and 678 nm), light absorption by colored dissolved and detrital matter at 412 nm (a_{dg}(412)) from the Garver-Siegel-Maritorena (GSM) model [Maritorena et al., 2002], sea surface temperature (SST), and normalized Fluorescence Line Height (nFLH). Here, we do not include nLw(λ) data from MODIS-Terra when doing analyses of all spectrum of radiance as most blue bands can be highly biased [Franz, et al., 2007]. The MODIS-Terra and MODIS-Aqua nLw(555) fields were merged in order to produce daily composites with increased data available. These daily composites were used in combination to the glider observations for identifying match-up periods with and without the CR plume influence. MODIS images of a_{dg}(412) and SST were used in the computation of a synthetic salinity product [Palacios et al., 2009]. All images are mapped in a cylindrical projection.

<u>Wind, river discharge and sea level data</u>
Daily river discharge data were obtained from USGS Oregon Water Science Center at the Beaver Army Terminal, Quincy, Oregon (http://waterdata.usgs.gov/usa/nwis/uv?site_no=14246900), whereas hourly data of wind speed and direction for buoy 46050 (Fig. 1) were obtained from the NOAA National Data Buoy Center (NDBC) website (http://www.ndbc.noaa.gov). Neutral wind stress was computed following Large and Pond [1981]. Wind data were low-pass filtered with a half-power point of 40 hours. The upwelling seasons (spring-summer) were limited from the spring to fall transition of each year according to the cumulative wind stress curve [Pierce et al., 2006]. We also computed the adjusted sea level (ASL) in order to confirm the drop in coastal sea level as response to the upwelling process [Kosro et al., 2006]. The coastal water level and atmospheric pressure data for the computation of the ASL were obtained from the tide gauge nearby Southbeach (http://tidesandcurrents.noaa.gov) and the NDCB station NWPO3 at Newport, respectively.

Results
The optical characteristics of the CR plume are highly distinct from adjacent ambient waters as seen in the MODIS imagery (Fig. 1). Its green-brownish color permits to track the plume southward for a large distance. This example is a fairly common pattern for the offshore CR plume and its signature is captured in the box of glider sampling. The high signal of the nLw(555) corroborates the southward extension of the plume during this event which was preceded by upwelling-favorable wind stress for 5 days and high river discharge (~11,860 m^3 s^{-1}). Also, contrasting spectral shapes exist among the near-field, far-field, and the further offshore ocean without the influence of the plume (Fig. 1c). Plume signatures present a higher nLw(λ) at the green bands whereas clear offshore waters peak at the lower part of the spectrum. The far-field plume presents higher nLw (less water absorption) at the blue bands than the near-field plume for this particular example (Fig. 1c).
Our cross-shore glider transects recorded many of these events through the 7 years of study, however, here we only present results from the glider trajectories that are concordant with clear MODIS nLw(555) fields identifying both the presence and absence of the CR plume. The MODIS imagery also revealed that some events with low salinity water were consistent to the signal from the small local rivers of central Oregon. Thus glider data suggesting the presence of the CR plume but not supported by a clear MODIS signature were discarded in order to avoid the inclusion of glider data under the influence of these small rivers. Two examples of glider transects under different river discharge conditions and recording the influence of the CR plume off Newport are presented in Fig. 2. The upwelling state characterized by several days with southward wind stress promotes the southward and offshore advection of the plume through the upwelling season. As it is expected high (low) river discharge early (late) in the upwelling season produces a plume with surface salinity values < 30 (~31.5-32.5) off Newport. In both cases the thickness of the plume spans ~20 m. The temperature field in the plume is higher in summer (Fig. 2f). As result, the plume is fresher (less fresh) and less warm (warmer) early (later) in the upwelling season. In general, the optics of the surface layer (0-20 m)

shows high backscatter and CDOM as compared to deeper levels. CDOM, however, seems to present a more coherent distribution with the low salinity water than the backscatter. High CDOM concentration also appears near the bottom (but lower than in the plume) and reaching the surface on the inner shelf (Fig. 2i,j). Finally, high chlorophyll fluorescence characterizes the plume and is extended to the surface at the frontal boundary between the inner part of the plume and the upwelling front (according to the salinity field) (Fig. 2k,l).

In order to evidence the contrasting optical characteristics between the offshore CR plume and ambient waters in the region, match-up between glider measurements and MODIS nLw(555) imagery were identified for both the presence of the CR plume and the absence of any turbid plume affecting the properties of ambient waters (Fig. 3). The presence of the plume, which shows a clear southward extension along most of the Oregon coast (Fig. 3a), is associated to a fresher and warmer surface (~20 m) layer, with high CDOM, backscatter, chlorophyll and oxygen concentrations. The buoyant character of the plume is illustrated through the T-S curves where the CR plume case is extended on average until the ~23 kg m^{-3} isopycnal, whereas the average curve for the case without the plume only reaches the ~25 kg m^{-3} isopycnal (Fig 3c). From the average profiles (curves in bold) it is possible to infer that the plume has some influence even below the surface 20 m of depth, considering that the CDOM profiles is minimum around 35-40 m (Fig. 3g). It is also important to note that besides the clear high signal of CDOM and backscatter in the surface layer, the CR plume case presents a surface peak in chlorophyll which is shallower than the case without the CR plume (Fig. 3i). This pattern is also shown in the dissolved oxygen of the surface 10 m (Fig. 3f).

To further explore the relation of optical conditions to salinity during spring-summer, multivariate regression analyses [Emery and Thompson, 2004] were performed between glider salinity (at different layers) and surface optical data from the gliders, MODIS nLw(λ), and MODIS $a_{dg}(412)$ (Fig. 4). The later one has been successfully used to predict surface salinity in the near-field plume [Palacios, et al., 2009]. As the plume shows a strong temperature signal, SST is also included in the analyses. In most cases, the inclusion of SST improves the prediction of salinity, specially in the surface layers (up to 10-15 m). Also, higher r^2 were obtained in spring than in summer (Fig. 4 upper panels vs lower panels). Optical data from gliders showed high relation to surface salinity as it is expected from figures 2 and 3. The inclusion of temperature produced better predictions of salinity mostly in the first 10 m. A sharp drop in the relation of surface (0-5 m) optics with deeper salinity layers existed (Fig. 4a,d). A similar pattern occurred when using the optics from MODIS. Surprisingly though the inclusion of SST improved the regression model not only in the first 10 m but also in deeper layers in spring (Fig. 4b). The r^2 curves from MODIS nLw(λ) were very similar to those using only glider data in summer (Fig. 4e), which enhances the use of multiple nLw(λ) for characterizing the low-salinity CR plume. Finally, salinity predictions using MODIS $a_{dg}(412)$ layers presented the lowest r^2 for both spring and summer (Fig. 4c,f). These results demonstrate that the optical characteristics of the offshore CR plume are better represented by using several wavelengths from MODIS, and that single channel CDOM-based synthetic salinity (prediction using $a_{dg}(412)$) do not work properly as in the near-field. Also, the drop in r^2 at around 15-20 m depth is coherent with the thickness of the plume during the upwelling season. The resultant 11 regression coefficients (β) from the regression model using surface (0-5 m) glider salinity and MODIS nLw(λ) + SST are used to compute MODIS-derived surface salinity fields for all match-up images and the average composites are presented for both CR plume and no-CR plume cases (Fig. 5). The southward extension of the CR plume is evident with salinities < 32. The inshore signal from the upwelling with higher salinity values (> 32) is also reproduced in HB, and placing the plume further offshore (Fig. 5a). For the case without the presence of the CR plume (Fig. 5b), the average MODIS-derived salinity field presents values > 32.5 in the region off Newport and there is no clear signal of the offshore CR plume (Fig. 5b). A re-sampling of the match-up data between MODIS and glider profiles, but now using the MODIS-derived salinity fields and the surface (0-5 m) glider salinity, reveal that the multivariate regression model overestimate the surface salinity in the fresher part of the salinity range (Fig. 6), but in general good prediction of fresh offshore CR plume waters can be done using this simple procedure. A new assessment of the MODIS-derived surface salinity with other source of surface salinity data (i.e. mooring off Newport) will be included in the final version of this paper.

Discussion

The influence of the CR plume off Oregon during spring-summer have mainly been described for the near-field region [Hickey et al., 2010, and references therein]. The plume play crucial role supplying nutrients during periods of delayed upwelling, maintaining high rates of primary productivity in new plume waters and enhancing zooplankton aggregations at the plume fronts [Hickey et al., 2010]. The impact of the plume on the far-field ecosystem, however, is practically unknown. Our glider average profiles suggest that the plume produces a shallower mixed layer, and consequently chlorophyll biomass presents a shallower peak than for the case without the CR plume (Fig. 3). The source of nutrients for this higher chlorophyll biomass is likely from the upwelling and very reduced or null from the river flow. The sections of chlorophyll fluorescence suggest the inner front of the plume (in conjunction to the upwelling front) would play an important role in promoting high surface chlorophyll (Fig. 2k,l). The fact that the offshore plume is well developed under strong/persistent upwelling conditions does not permit to separate the influence of the plume from the upwelling. Maps of nFLH confirm the presence of high chlorophyll in costal waters off Oregon during active upwelling and with the presence of the plume (Fig. 7a). In contrast, the case without the CR plume, mostly during wind reversals, show a more disperse chlorophyll activity with higher values offshore and reduced chlorophyll activity over HB (Fig. 7b). Future studies using a biophysical model would better address the role of the plume (upwelling with CR plume vs upwelling without the CR plume) in the chlorophyll dynamics off Oregon.

The change in optical properties as the plume is transported southward [Pak et al., 1970] can be evidenced from the differences in the spectral shape curves between the near-field and far-field plumes (Fig. 1c). The differences in nLw(λ) at the blue bands (400-450 nm) would resemble the decreased influence of CDOM in the far-field (less water absorption at these bands) as compared to the near-field. Lower nLw(λ) at the green bands would also suggest that the amount of suspended material is also reduced (Fig. 1c). The decreased level of turbidity of the far-field plume as compared to the near-field plume has implications in the processing procedure of nLw(λ). The higher values of nLw(748) in the near-field plume suggest a considerable influence of high sediment concentrations on the quality of ocean color products as the black pixel assumption does not longer hold [e.g. Wang and Shi, 2005]. Consequently, SWIR bands would be more suitable for atmospheric correction in the near-field plume. The unique character of the optical properties of the offshore CR plume in spring-summer permits a clear identification of plume waters when using MODIS imagery. The multi-channel approach demonstrated to be a better option for mapping the influence of the plume on coastal waters. In fact, key differences in the spatial distribution of nLw(555) and the MODIS-derived surface salinity field also suggest that the plume's optics is too complex to be represented using a single channel as in other studies [Thomas and Weatherbee, 2006; Palacios et al., 2009]. A clear example is the poor representation of the plume extended offshore and partially detached from the coast from the nLw(555) field (Fig. 3a), whereas the MODIS-derived surface salinity shows a more coherent plume detached from the coast off Newport and interacting with the topography (Fig. 5a). The over-prediction of the MODIS-derived salinity, nonetheless, rise the question if other more sophisticated statistical approaches, as cluster analysis [e.g. Palacios et al., 2012] or neural network models [e.g. Geiger et al., 2013], would produce better predictions for the far-field offshore CR plume. Future studies should consider these approximations and incorporating surface salinity data from different locations in the alongshore direction.

It is well known that the visible bands from MODIS present different level of noise, and therefore the

total number of match-up data for the regression analyses varies depending of the bands considered in the analysis. In a linear multivariate regression model the addition of coefficients (adding more variables) will intrinsically increase the skill, but if the number of data points included in the analysis varies, then the skill could also decrease. In consequence, a maximum skill was searched as function of the number of regression coefficients (Fig. 8). These results show that is not necessary to process all 10 nLw(λ) bands to produce a good estimation of surface salinity. The processing of only 6 nLw(λ) bands + SST produce a slightly better estimate during spring and basically the same result for summer (see table 1 for identifications of these bands), which decrease considerably the processing time of MODIS imagery and computational power necessary for achieving the best prediction of salinity.
Future work including additional glider data from the Ocean Observing Initiative (OOI) glider endurance lines (Fig. 8a; yellow lines) will improve the spatial cover of our sampling and would produce a more robust relation between plume's salinity and MODIS nLw(λ) for the whole domain.

Conclusions

- 7 years of glider measurements off Oregon reveal the optical characteristics of the offshore CR plume during spring and summer. The plume is characterized by presenting high CDOM, backscatter and chlorophyll fluorescence.
- The thickness of the plume is around 20 m according to salinity, which produces a shallower maxima in chlorophyll as compared to the cases without the presence of the plume.
- High chlorophyll fluorescence outcrop to the surface following the frontal boundary between the inner part of the plume and the upwelling front.
- A comparison of regression analyses between optics (from gliders and MODIS) and glider salinity layers reveal similar skill curves for the surface 45 m of the water column, which enhances the use of MODIS imagery matching glider data.
- Composites of MODIS-derived surface salinity from the best regression estimates using MODIS visible nLw(λ) produce more coherent low salinity plume fields than tracking the plume from a single MODIS band as in previous studies. This salinity prediction is overestimated for the fresher part of the salinity range.
- Maps of nFLH for the cases of active upwelling with the presence of the CR plume show high chlorophyll activity over shelf waters, and particularly over Heceta Bank.
- Due to the higher noise of some blue bands of MODIS, the number of data points including in the regression analysis changes as function of the number of regression coefficients, and an optimum prediction of surface salinity is mostly accomplish by processing around 6 nLw(λ) + SST.

References

Barnes, C. A., A. C. Duxbury, B. Morse (1972), Circulation and selected properties of the Columbia River effluent at sea, in *The Columbia River Estuary and Adjacent Ocean Waters* (A. T. Pruter, D. L. Alverson, University of Washington Press, Seattle, WA).

Boss, E., and W. S. Pegau (2001), Relationship of light scattering at an angle in the backward direction to the backscattering coefficient, Appl. Opt. 40, 5503-5507.

Cetinić, I., G. Toro-Farmer, M. Ragan, C. Oberg, and B. H. Jones (2009), Calibration procedure for slocum glider deployed optical instruments, Opt. Express, 17, 15420-15430.

Del Castillo, C. E., P. G. Coble, J. M. Morell, J. M. López, and J. E. Corredor (1999), Analysis of the optical properties of the Orinoco River plume by absorption and fluorescence spectroscopy, Mar. Chem. 66(1), 35-51.

Emery, W. J., and R. E. Thomson (2004), Data Analysis Methods in Physical Oceanography, 2nd ed., Elsevier, Amsterdam.

Fiedler, P. C., and R. M. Laurs (1990), Variability of the Columbia River plume observed in visible and infrared satellite imagery, Int. J. Remote Sens., 11, 999-1010.

Franz, B. A., E. J. Kwiatkowska, G. Meister, and C. R. McClain (2007), Utility of MODIS-Terra for ocean color applications, Proc. SPIE.

Geiger, E. F., M. D. Grossi, A. C. Trembanis, J. T. Kohut, and M. J. Oliver (2013), Satellite-derived coastal ocean and estuarine salinity in the Mid-Atlantic, Cont. Shelf Res., 63, S235-S242.

Gordon, H. R. (1997), Atmospheric correction of ocean color imagery in the Earth Observing System era, J. Geophys. Res. 102, 17081-17106.

Hickey, B. M., et al. (2010), River influences on shelf ecosystems: Introduction and synthesis, J. Geophys. Res., 115, C00B17, doi:10.1029/2009JC005452.

Hickey, B. M., L. J. Pietrafesa, D. A. Jay, and W. C. Boicourt (1998), The Columbia River plume study: Subtidal variability in the velocity and salinity fields, J. Geophys. Res. 103(C5), 10339-10368.

Huyer, A., P. A. Wheeler, P. T. Strub, R. L. Smith, R. Letelier, and P. M. Kosro (2007), The Newport line off Oregon – Studies in the North East Pacific, Prog. Oceanogr., 75, 126-160.

Kosro, P. M., W. T. Peterson, B. M. Hickey, R. K. Shearman, and S. D. Pierce (2006), Physical versus biological spring transition: 2005, Geophys. Res. Lett. 33, L22S03, doi:10.1029/2006GL027072.

Kudela, R. M., et al., (2010), Multiple trophic levels fueled by recirculation in the Columbia River plume, Geophys. Res. Lett. 37, L18607, doi:10.1029/2010GL044342.

Large, W. G., and S. Pond (1981), Open ocean momentum flux measurements in moderate to strong winds, J. Phys. Oceanogr. 11(3), 324-336.

Maritorena, S., D. A. Siegel, and A. R. Peterson (2002), Optimization of a semi-analytical ocean color model for global-scale applications, Appl. Opt., 41, 2705-2714.

Milliman, J.D., and R.H. Meade (1983), World-wide delivery of river sediment to the oceans, J. Geol. 91, 1-21.

Morel, A. (1974), Optical properties of pure water and pure sea water, in Optical Aspects of Oceanography, N. G. Jerlov and E. S. Neilsen, eds. (Academic, New York, 1974) pp. 1-24.

Morgan, C. A., A. De Robertis, R. W. Zabel (2005), Columbia River plume fronts. I. Hydrography, zooplankton distribution, and community composition, Mar. Ecol. Prog. Ser. 299, 19-31.

Nowacki, D. J., A. R. Horner-Devine, J. D. Nash, and D. A. Jay (2012), Rapid sediment removal from the Columbia River plume near field, Cont. Shelf Res. 35, 16-28.

Pak, H., G.F. Beardsley, and P. K. Park (1970), The Columbia River as a source of marine light-scattering particles, J. Geophys. Res. 75, 4570-4578 (1970).

Palacios, S. L., T. D. Peterson, and R. M. Kudela (2009), Development of synthetic salinity from remote sensing for the Columbia River plume, J. Geophys. Res. 114, C00B05, doi:10.1029/2008JC004895.

Palacios, S. L., T. D. Peterson, and R. M. Kudela (2012), Optical characterization of water masses within the Columbia River plume, J. Geophys. Res. 117, C11020, doi:10.1029/2012JC008005.

Pierce, S. D., J. A. Barth, R. E. Thomas, and G. W. Fleischer (2006), Anomalous warm July 2005 in the northern California Current: Historical context and the significance of cumulative wind stress, Geophys. Res. Lett. 33, L22S04, doi:10.1029/2006GL027149.

Schofield, O., et al., (2007), Slocum gliders: Robust and ready, J. Field Rob. 24(6), 1-14.

Spahn, E. Y., A. R. Horner-Devine, J. D. Nash, D. A. Jay, and L. Kilcher (2009), Particle resuspension in the Columbia River plume near field, J. Geophys. Res. 114, C00B14, doi:10.1029/2008JC004986.

Thomas, A. C., and R. A. Weatherbee (2006), Satellite-measured temporal variability of the Columbia River plume, Remote Sens. Environ., 100(2), 167-178.

Wang, M., and W. Shi (2005), Estimation of ocean contribution at the MODIS near-infrared wavelengths along the east coast of the U.S.: two case studies, Geophys. Res. Lett., 32, L13606, doi:10.1029/2005GL022917.

Wang, M., and W. Shi (2007), The NIR-SWIR combined atmospheric correction approach for MODIS ocean color data processing, Opt. Express, 15(24), 15722-15733.

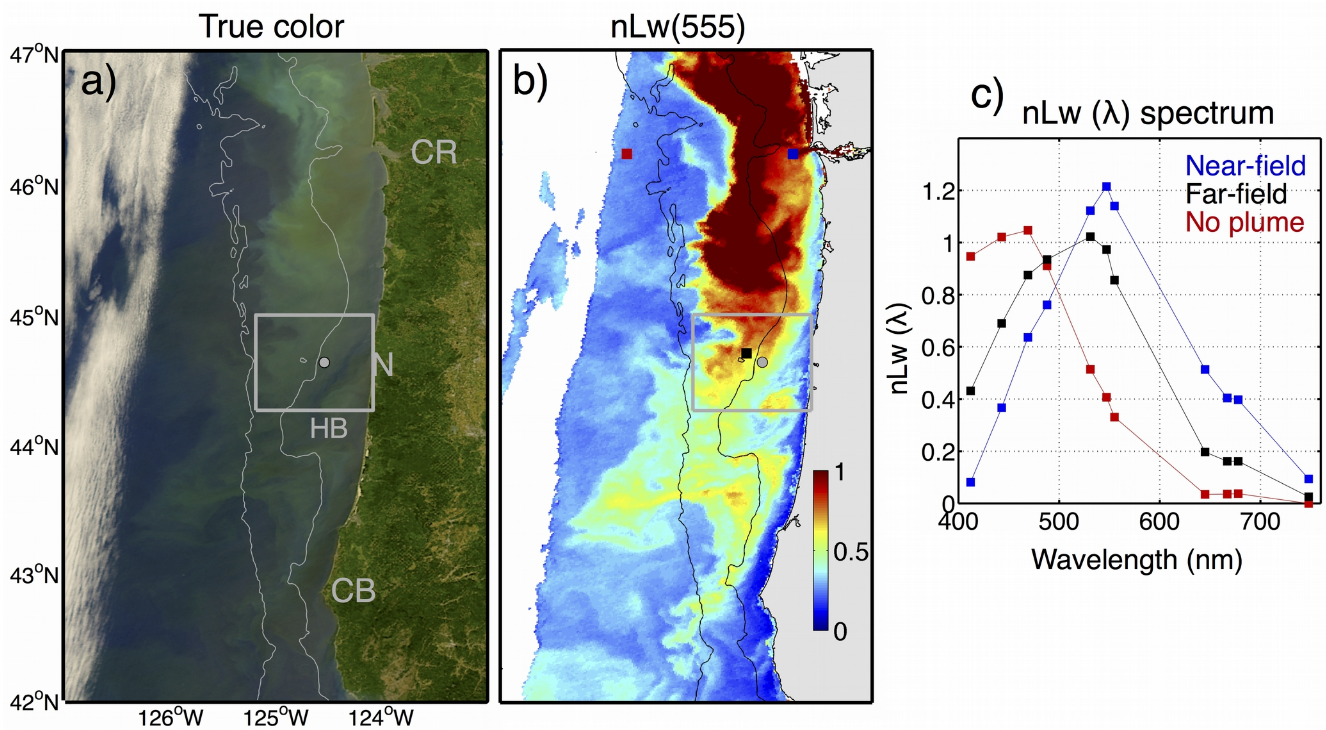

Figure 1. Study area in a MODIS-Aqua true color image (a) and its corresponding nLw(λ) signature at 555 nm (b), showing the CR plume off Oregon on June 27, 2008. The nLw(555) field has been normalized by the mean value at the CR mouth (5x10 km box). The grey box indicate the area for all glider trajectories during the upwelling seasons off Newport, Oregon, where low-salinity CR water has been recorded. The grey dot in the middle of the box represents the location of NDBC meteorological buoy 46050. Labels for Columbia River (CR), Newport (N), Cape Blanco (CB), and Heceta Bank (HB) are also included, and the 200 m and 2000 m isobaths are shown in grey lines. The nLw(555) has been previously shown to be an effective tracer of particulate matter from the river mouth [Thomas and Weatherbee, 2006]. The contrast of the true color image has been increased for a better visualization of the plume.

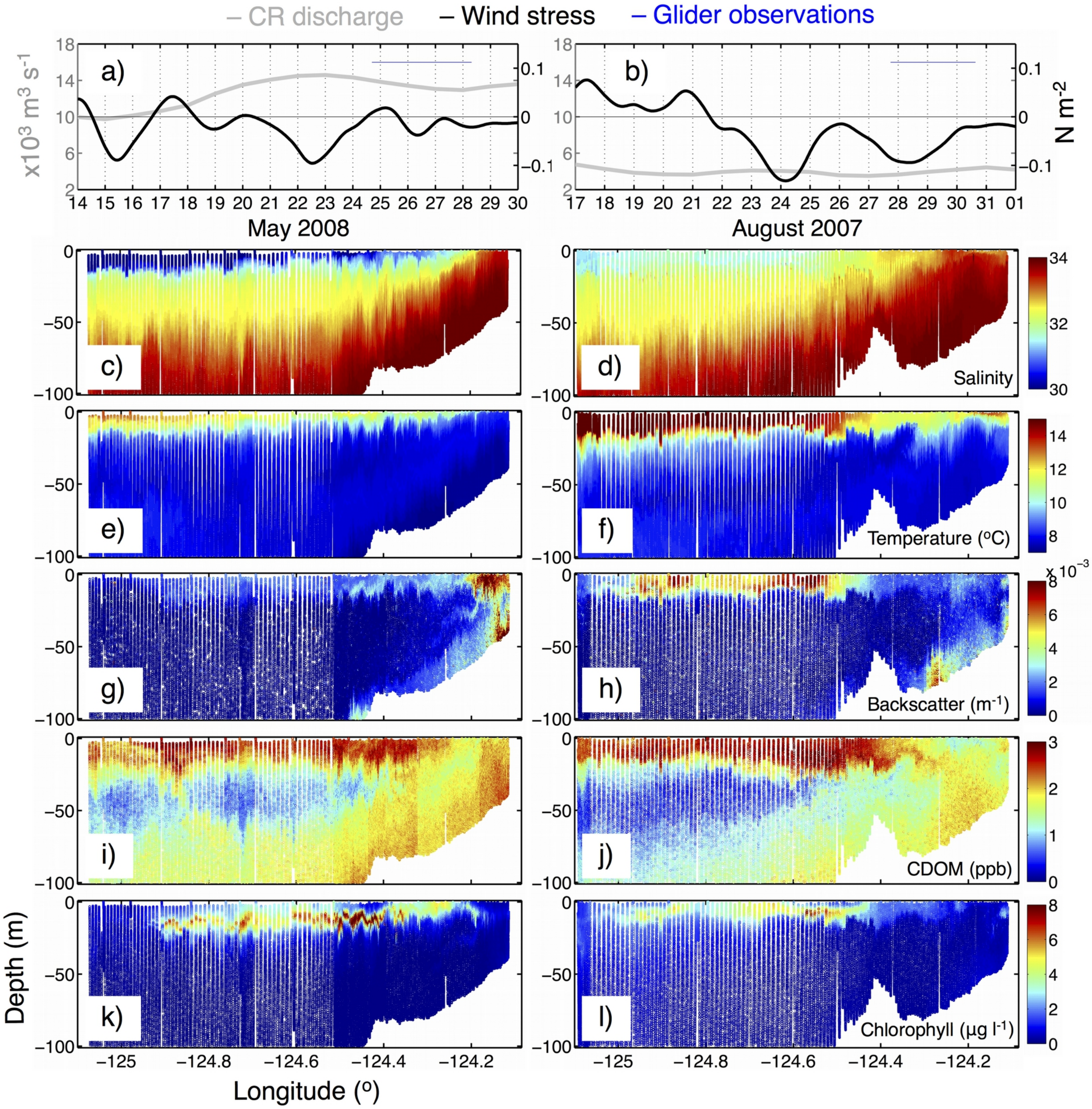

Figure 2. Examples of glider sections recording the presence of the CR plume off Oregon under contrasting river discharge conditions. Left (right) panels correspond to an event with high (low) river flow in relation to its annual cycle. River flow and wind stress data for previous days and during glider observations are shown in (a-b). Notice that the time of the glider observations are denoted with a blue line in (a-b). Glider data correspond to salinity (c-d), temperature (e-f), backscatter (g-h), CDOM fluorescence (i-j), and chlorophyll fluorescence (k-l).

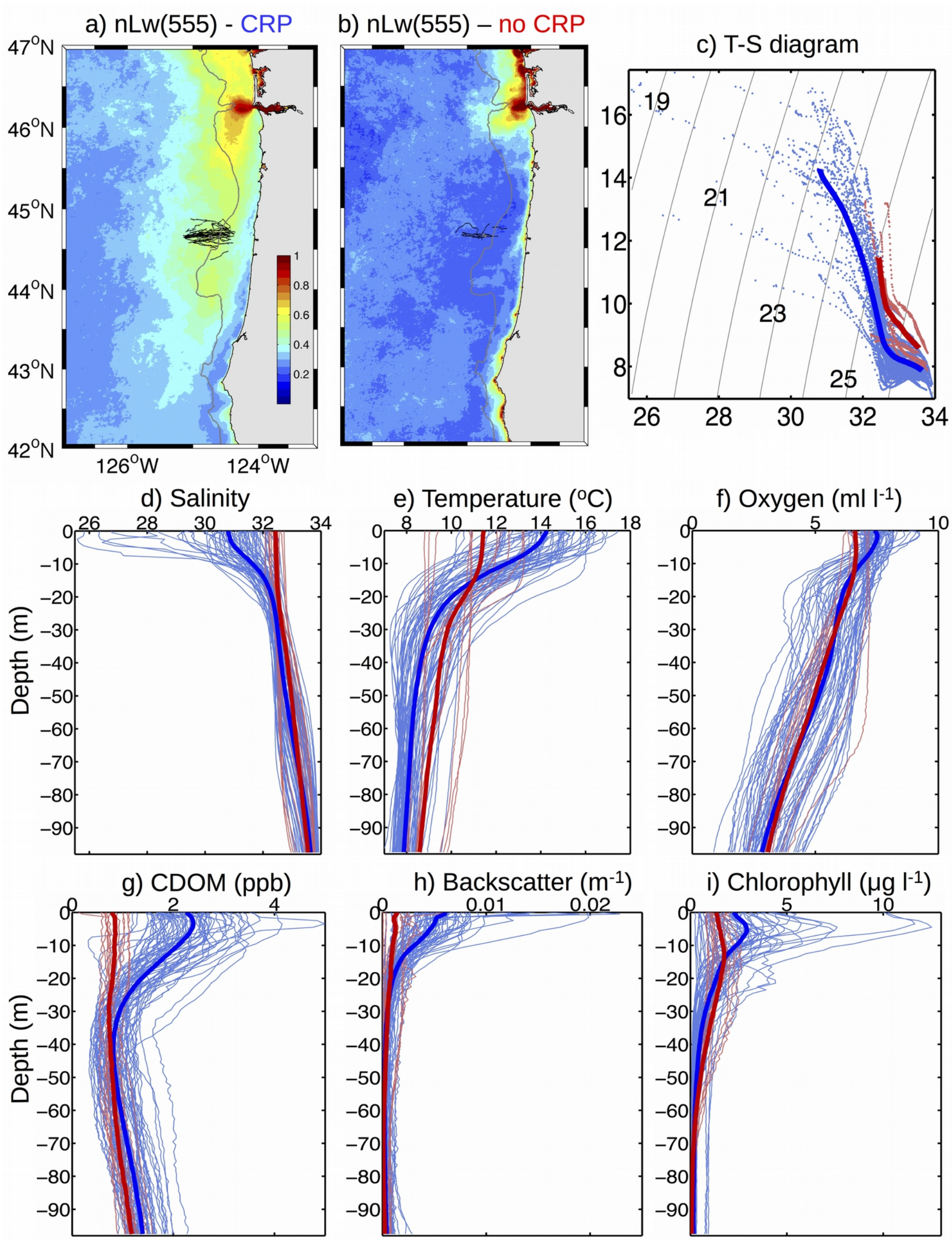

Figure 3. MODIS average nLw(555) imagery for match-up days with (a) and without (b) the presence of the CR plume off Newport. Glider trajectories for these days are included in both cases. All average daily profiles from matched glider measurements are presented in blue (with CR plume) and red (without CR plume) for each variable (d-i: Salinity, temperature, oxygen, CDOM, backscatter, and chlorophyll). profiles in bold are the average profile for all respective matches. A T-S diagram is also included for better representation of the water masses characterizing the presence and absence of the CR plume off Newport.

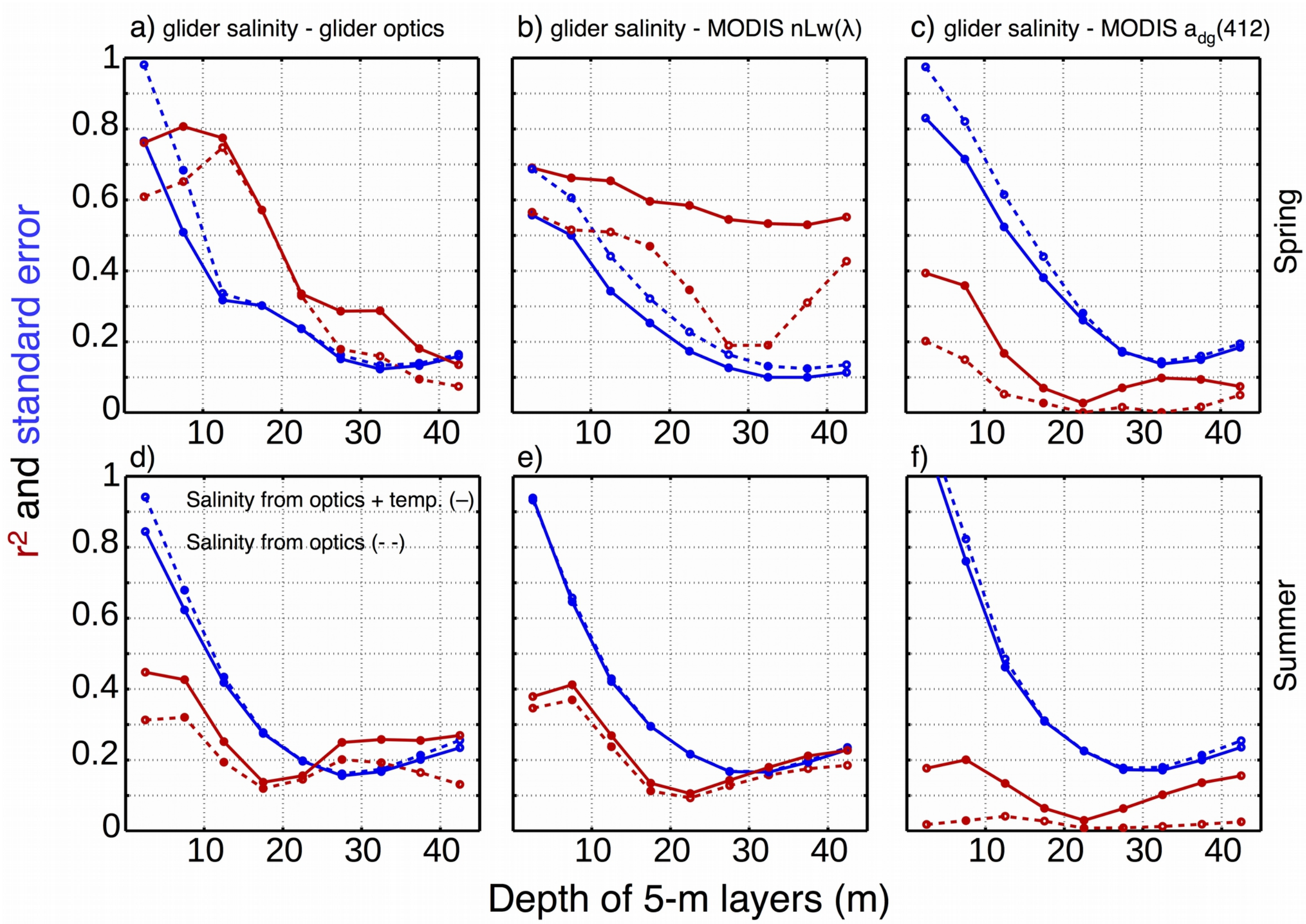

Figure 4. Results from regression analyses (skill and standard error) using all optics (dashed lines) and optics + SST (solid lines) from (a,d) gliders, (b,e) MODIS nLw(λ), and (c,f) MODIS $a_{dg}(412)$ for predicting glider salinity at different 5-m layers in spring (upper panels) and summer (lower panels).

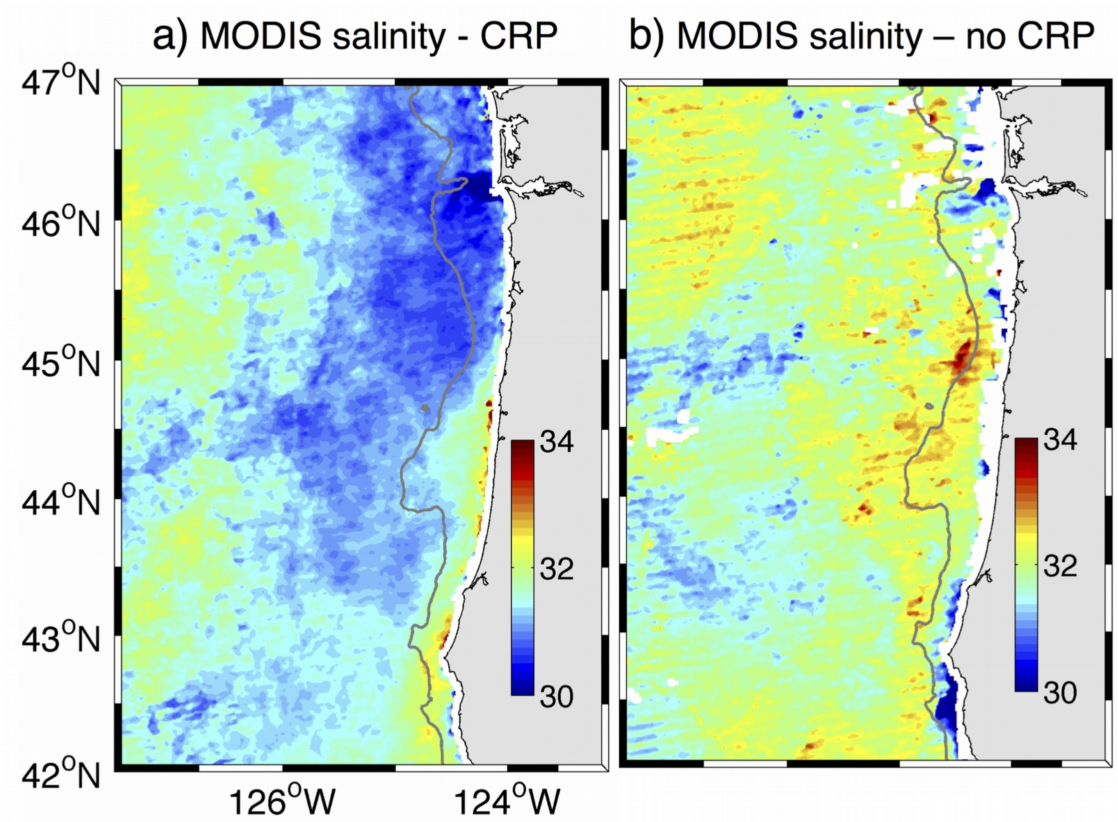

Figure 5. Average MODIS-derived surface salinity for MODIS match-up images corresponding to (a) the presence, and (b) absence of the CR plume. These are the same cases as in figure 3 (a) and (b).

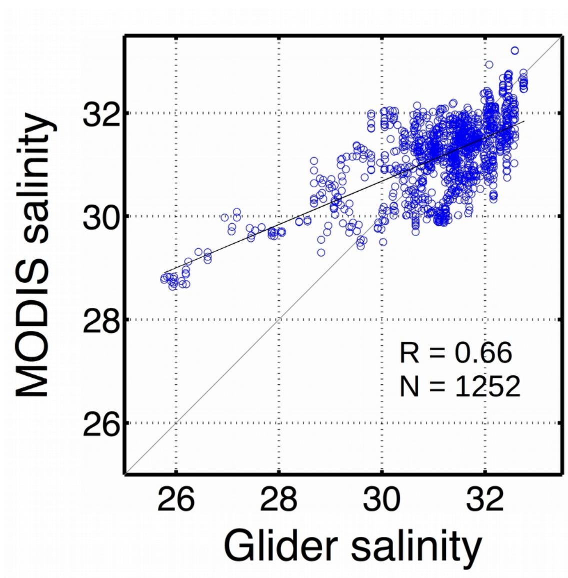

Figure 6. Correlation for all match-up data between MODIS-derived surface salinity and the surface (0-5 m) glider salinity.

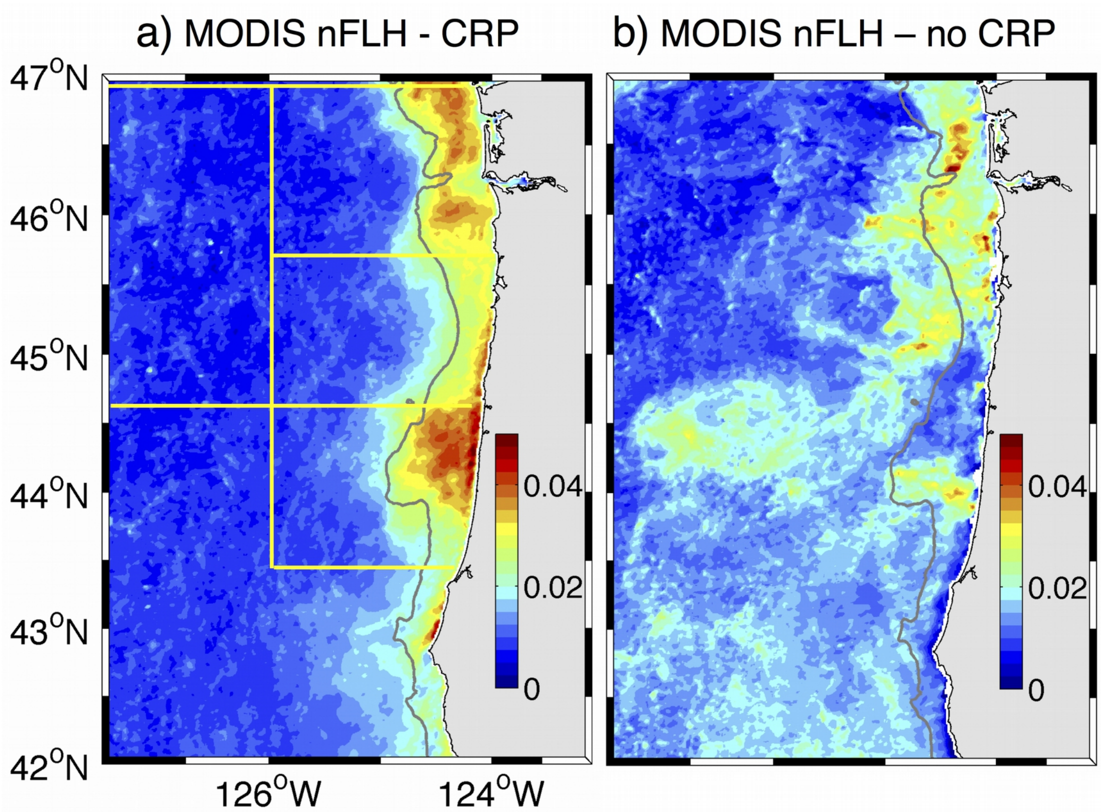

Figure 7. The same as in figure 5 except for normalized Fluorescence Line Height (nFLH). Yellow lines in (a) indicate proposed glider trajectories for Ocean Observing Initiative (OOI) endurance array.

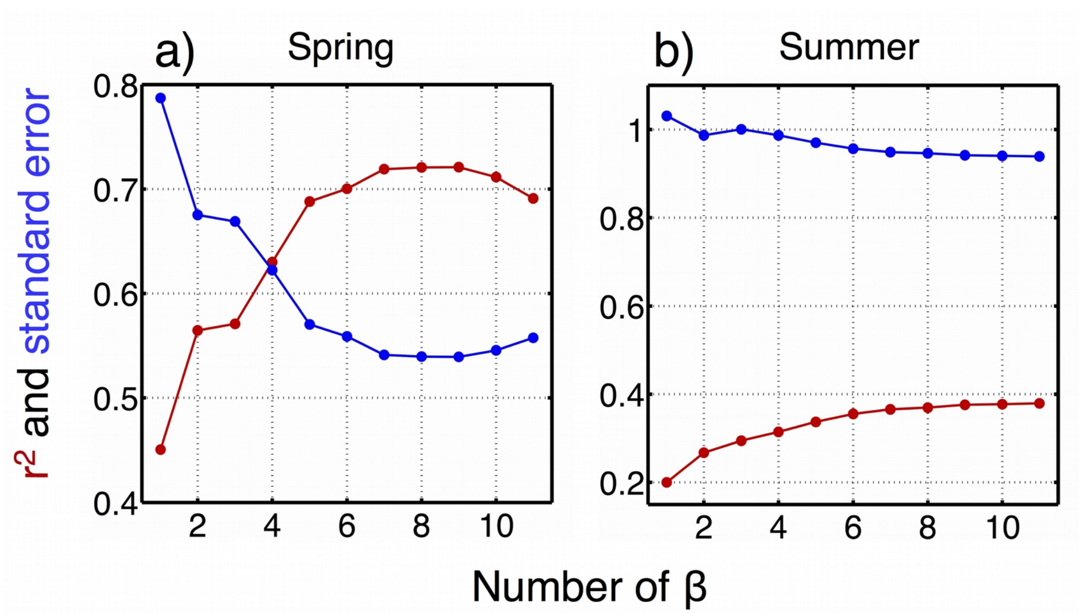

Figure 8. Maximum skill (r^2) and standard error for multivariate regression analyses between MODIS nLw(λ) and surface (0-5 m) glider salinity as function of the number of regression coefficients (β) included for spring and summer. The MODIS bands and SST producing the maximum skills are presented in table 1.

Table 1. Combination of nLw(λ) bands and SST required for producing the best skill (r^2) in multivariate regression models as varying the number of regression coefficients (β) for spring (x) and summer (+). N is the total number of possible combinations for each case.

	412 nm	**443 nm**	**469 nm**	**488 nm**	**531 nm**	**547 nm**	**555 nm**	**645 nm**	**667 nm**	**678 nm**	**SST**	**N**
2 β		x		+								11
3 β	+	+	x								x	55
4 β	+	+					x			x	x +	165
5 β	+	+	x		x +		x				x +	330
6 β	+	+		x	x	+	x		+	x	x +	462
7 β	+	+		x	x +	x	x		+	x +	x +	462
8 β	+	+		x	x +	x	x	x +	+	x +	x +	330
9 β	+	+	x	x	x	x +	x +	x +	+	x +	x +	165
10 β	+	x +	x +	x	x +	x	x +	x +	+	x +	x +	55
11 β	+	x +	x +	x	x +	x +	x +	x +	x +	x +	x +	11
12 β	x +	x +	x +	x +	x +	x +	x +	x +	x +	x +	x +	1